Self-assembled quantum dots with tunable thickness of the wetting layer: Role of vertical confinement on interlevel spacing

Lijuan Wang,[1,*] Vlastimil Křápek,[2] Fei Ding,[1,2] Felicity Horton,[1] Andrei Schliwa,[3] Dieter Bimberg,[3] Armando Rastelli,[2,†] and Oliver G. Schmidt[2]

[1]*Max-Planck-Institut für Festkörperforschung, Heisenbergstrasse 1, D-70569 Stuttgart, Germany*

[2]*Institute for Integrative Nanosciences, IFW Dresden, Helmholtzstrasse 20, D-01069 Dresden, Germany*

[3]*Institut für Festkörperphysik, Technische Universität Berlin, Hardenbergstrasse 36, 10623 Berlin, Germany*

(Received 5 May 2009; revised manuscript received 7 July 2009; published 18 August 2009)

Epitaxial self-assembled quantum dots (QDs) are commonly obtained by the Stranski-Krastanow (SK) growth mode, in which QDs form on top of a thin two-dimensional (2D) wetting layer (WL). In SK QDs, the properties of the WL such as thickness and composition are hard to control independently of those of the overlying QDs. We investigate here strain-free GaAs/AlGaAs QDs located under a GaAs quantum well (QW), analogous to the WL in SK QDs. The thickness of such a QW can be arbitrarily controlled, allowing the optical properties of the QDs to be tuned without modifying the QD morphology and/or composition. By means of single-QD photoluminescence spectroscopy, we observe well-resolved excited-state shell structures with intershell spacing increasing monotonically with decreasing QW thickness. This behavior is well reproduced by eight-band $k \cdot p$ calculations combined with the configuration-interaction model taking the realistic QD morphology as input. Furthermore, for the thinnest GaAs layer investigated here, no QW emission is detected, indicating that it is possible to suppress the two-dimensional layer usually connecting QDs. Finally, we find that all recombination involving an electron-hole pair in the ground state, including the positive trion, occurs at the low-energy side of the neutral exciton emission. This behavior, previously observed for GaAs/AlGaAs QWs, is a consequence of the large lateral extent of the QDs, and hence of pronounced self-consistency and correlation effects.

DOI: 10.1103/PhysRevB.80.085309 PACS number(s): 81.07.Ta

I. INTRODUCTION

Semiconductor quantum dots (QDs), also referred to as "artificial atoms," can be conveniently fabricated by self-assembled epitaxial growth. For the realization of QD-based devices, the optical properties of the QDs such as the emission wavelength, the intersublevel spacing energy, the ensemble homogeneity, and even the interactions between nearby QDs should be free for engineering. The most common method to obtain high quality QDs consists in exploiting the Stranski-Krastanow (SK) growth mode during strained heteroepitaxial growth, in which QDs spontaneously form on top of a thin wetting layer (WL). An example is InAs QDs on GaAs(001) substrate. The structural properties of such QDs, such as size, shape, and composition, can be controlled to some extent by varying the growth parameters during InAs deposition. Alternatively, the QD structure can be tuned *in situ* by partial capping and annealing[1,2] or by *ex situ* post-growth rapid thermal annealing.[3–5] Both the transition energies and the intersublevel spacing energies can be adjusted by the above methods either through a reduction in QD height or by promoting In-Ga intermixing, which reduces the QD confinement potential. In both cases, the shape, size, and composition profile of QDs vary during the tuning processes.

In SK QDs, the thickness of the WL can only be controlled in a narrow range, because it is mainly governed by the misfit strain between deposited material and substrate material.[6] On the other hand, unstrained QDs offer the possibility of independent tuning of WL thickness and QD shape/size. Self-assembled unstrained GaAs/AlGaAs QDs can be fabricated by local droplet etching[7] or by modified droplet epitaxy (MDE).[8] With the latter method GaAs QDs on top of a GaAs quantum well (QW) with arbitrary thickness can be obtained. In analogy to SK QDs, we refer to the QW as "WL." The effect of the GaAs WL thickness on the emission of QDs was investigated in Ref. 8 by photoluminescence (PL) spectroscopy. It was shown that a decrease in the WL thickness produces a blueshift in the ground-state (GS) emission and the WL can even be completely suppressed. However, no appreciable effect on the separation between GS and excited-state (ES) emission was observed, possibly because the PL inhomogeneous broadening prevented the observation of well-resolved excited-state "shells."

To eliminate the effect of inhomogeneous broadening we investigate here the light emission of single GaAs/AlGaAs QDs fabricated by "hierarchical self-assembly" (Refs. 9 and 10) as a function of WL thickness. These QDs are defined by filling $Al_{0.45}Ga_{0.55}As$ nanoholes with GaAs with variable thicknesses. Therefore, in contrast to SK and MDE QDs, this growth technique creates inverted GaAs QDs inside $Al_{0.45}Ga_{0.55}As$ holes with a QW (or WL) above the QDs. By depositing small amount of GaAs, the formation of the WL can also be fully suppressed.

Different from commonly investigated SK InAs/GaAs QDs and independent of WL thickness, we find that all optical transitions involving the recombination of a ground-state electron with a ground-state hole, including the positive trion (X^+), are characterized by energies lower than the neutral exciton (X). This behavior is well reproduced by an

eight-band $k \cdot p$ calculation combined with the configuration-interaction model.

Although the shape and lateral extent of the QDs are kept nominally fixed, a reduction in the WL thickness, and hence of the QD height, produces a systematic increase in the GS-ES energy separation. This observation can be seen as a "cross talk" between vertical confinement potential and lateral confinement potential, responsible for the GS-ES splitting. The observed behavior is qualitatively explained with a simple model and quantitatively reproduced by eight-band $k \cdot p$ calculations combined with the configuration-interaction model.

II. EXPERIMENTAL METHODS

The samples studied here were grown by a solid-source molecular-beam epitaxy (MBE) machine equipped with an $AsBr_3$ gas etching unit. A layer of InAs QDs grown on GaAs (001) at a nominal substrate temperature of 500 °C was the starting point for the fabrication of GaAs/AlGaAs QDs. The as-grown InAs QDs were overgrown with 10 nm GaAs and nominal 5-nm-deep $AsBr_3$ etching was applied *in situ*. As a result of the strain-enhanced and material-selective etching rate, bow-tie-shaped nanoholes were created by etching away the buried InAs QDs.[11,12] To create the lower barrier for the QD confinement potential, the obtained GaAs nanoholes were overgrown with 10 nm $Al_{0.45}Ga_{0.55}As$. Due to the low diffusivity of $Al_{0.45}Ga_{0.55}As$ on the GaAs surface, the nanoholes are preserved after the overgrowth. The obtained $Al_{0.45}Ga_{0.55}As$ nanoholes were filled immediately by depositing GaAs of variable thicknesses followed by a one min growth interruption at 500 °C, which allows the diffusion of the GaAs into the nanoholes. This multistep growth leads to the formation of inverted GaAs QDs with tunable QD height and WL thickness.

In order to deduce the morphology and size of the GaAs QDs, the morphology of the $Al_{0.45}Ga_{0.55}As$ nanoholes and uncapped GaAs QDs was studied by atomic force microscopy (AFM) in tapping mode at room temperature. For AFM characterization we employed samples with relatively high surface density of QDs ($\sim 10^9$ cm^{-2}) to collect large statistical information from small area images. For PL characterization of single QDs we used low-density ($\lesssim 10^8$ cm^{-2}) QD samples to avoid using shadow masks. The density was simply tuned by adjusting the amount of deposited InAs. We previously verified that the QD density has negligible effects on the emission energy of the GaAs/AlGaAs QDs, which is a consequence of the fact that we use dome-shaped InAs QDs (Ref. 13) with similar sizes independent of density. We can thus safely use the AFM data to model the optical properties of samples studied by PL spectroscopy.

For PL investigations, the GaAs QDs were buried by 100 nm $Al_{0.35}Ga_{0.65}As$, 20 nm $Al_{0.45}Ga_{0.55}As$, and 10 nm GaAs. The PL spectroscopy of single QDs was performed in a standard micro-PL setup at 6 K by using a laser emission of 532 nm as an excitation source, and a spectrometer with 500 mm focal length equipped with a charge-coupled device for detection.

III. THEORETICAL MODELING

To gain insight into the electronic structure and optical properties of the studied QDs we calculated transition energies of various excitonic complexes confined in QDs. The following two-step process was used: first, we obtained single-particle states using eight-band $k \cdot p$ theory.[14] Second, we performed configuration-interaction (CI) calculations, in which the multiparticle states are expanded into a series of Slater determinants (SDs) constructed from the single-particle states.[15]

The eight-band $k \cdot p$ theory presents an efficient way to obtain the electronic structure with very good accuracy and at acceptable computational expenses. It accounts for the conduction and valence-band mixing, while the effects of strain and piezoelectric field are not considered in this paper due to the negligible lattice mismatch between GaAs and AlGaAs. A numerical implementation consists in the finite difference scheme, which allows for a convenient treatment of arbitrary shape of QDs. The details of the implementation are given elsewhere.[14,16]

In the simulation the QDs are made of pure GaAs, since we expect limited interdiffusion of Al and Ga in the QDs at the low substrate temperature used in the experiment. The bottom surface of the QDs is determined from AFM measurements performed on the unfilled $Al_{0.45}Ga_{0.55}As$ nanoholes. The upper surface of the QDs is assumed to be flat. Although in the experiment a perfectly flat GaAs surface is not recovered after one min annealing (see below), we should point out that the real thickness of the QDs cannot be accessed by AFM measurements and it can only be estimated from the amount of the deposited GaAs d. Due to this uncertainty in the QD height and unavoidable uncertainty in the exact size/shape of the dots investigated by PL spectroscopy, we substitute the realistic profile of the top surface revealed by AFM by a simple plane. Such a treatment is reasonable since a rather flat profile is observed at the center of the filled holes, where the high electron probability occurs. Therefore, a flat top surface is adopted and an adjustable parameter h is introduced in our model, which represents the height of the top plane above the AlGaAs nanohole plane. This parameter roughly corresponds to the nominal WL thickness d. The structure is subsequently discretized for the finite difference calculations. With a grid step of 0.5 nm, a typical grid consists of $120 \times 120 \times 40$ points.

The multiparticle Hamiltonian consists of a sum of single-particle Hamiltonians and Coulomb interaction terms. Approximately, the wave function of a multiparticle complex can be constructed as a SD of single-particle states. However, such a wave function is not the eigenstate of the multiparticle Hamiltonian because the single-particle wave functions are deformed by the mutual Coulomb interaction. This effect is treated within CI by expanding the wave function into a series of SDs. In our calculation we used ten electron and ten hole wave functions, resulting in 100 SDs for the neutral exciton, 450 for the trions, and 2025 for the neutral biexciton.

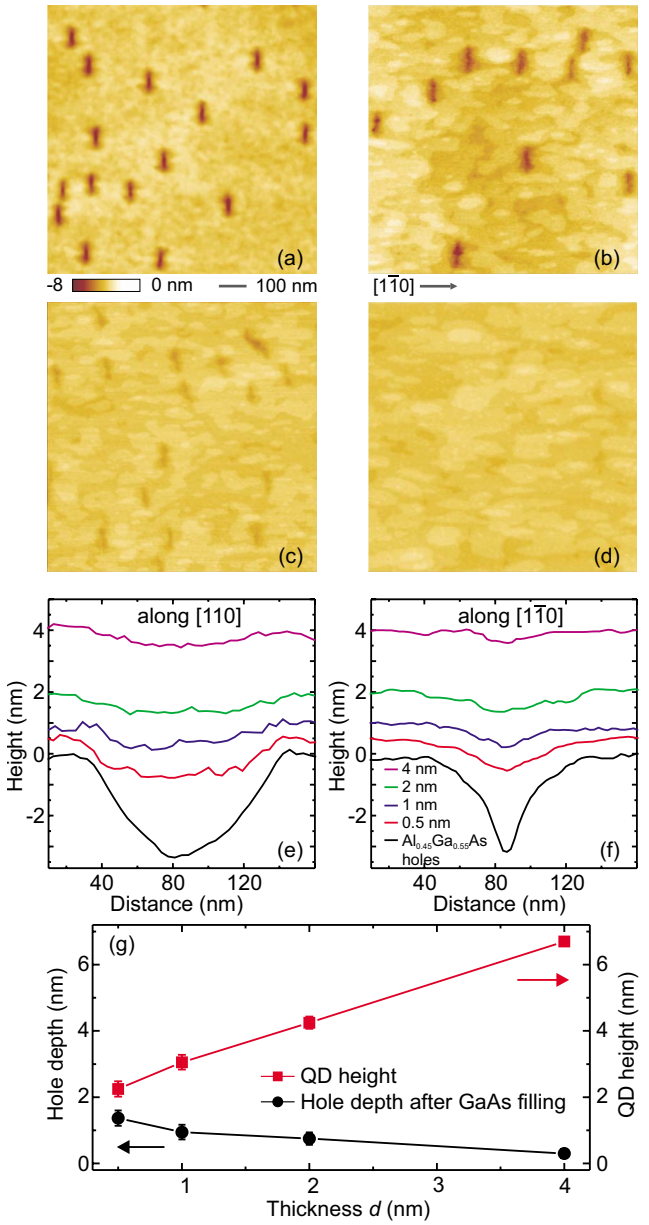

FIG. 1. (Color online) AFM image of $Al_{0.45}Ga_{0.55}As$ nanoholes (a) and of nanoholes filled with GaAs with nominal thickness d of (b) 0.5 nm, (c) 1 nm, and (d) 4 nm followed by one min annealing prior to cooling to room temperature. Linescans of representative nanoholes in the (e) [110] and (f) [1$\bar{1}$0] directions. The lines are offset in vertical direction by an amount equal to d. (g) Depth of the GaAs-filled nanoholes and the deduced height of GaAs QDs for different GaAs fillings. The QD height for each sample is extracted from the difference in depth for the $Al_{0.45}Ga_{0.55}As$ nanoholes and the GaAs-filled nanoholes plus d.

IV. RESULTS AND DISCUSSION

A. Morphology of GaAs/AlGaAs quantum dots

In order to determine the morphology of the GaAs QDs, we imaged by AFM the bottom and the top interfaces with the $Al_{0.45}Ga_{0.55}As$ and $Al_{0.35}Ga_{0.65}As$ barriers, respectively. Figure 1(a) shows an AFM image of $Al_{0.45}Ga_{0.55}As$ nanoholes created by overgrowing the GaAs nanoholes with 10 nm $Al_{0.45}Ga_{0.55}As$. The holes have an average depth of about 3 nm [see Figs. 1(e) and 1(f)] and are elongated in the [110] direction, similar to previous results.[10] The hole depth rapidly decreases as more GaAs is deposited on the AlGaAs surface followed by annealing [Figs. 1(b)–1(d)]. This is due to GaAs diffusion inside the holes driven by the local positive surface curvature. The surface evolution is better seen in Figs. 1(e) and 1(f), where linescans of representative $Al_{0.45}Ga_{0.55}As$ and GaAs-overgrown nanoholes are displayed together along the [110] and [1$\bar{1}$0] crystal directions. Linescans are vertically shifted by an amount d (WL thickness), to illustrate the QD plus WL morphology and size in cross section. From the linescans we see that nanoholes are completely filled with GaAs already for $d=0.5$ nm. On the other hand, the surface above the GaAs QDs is atomically smooth only for $d\sim 4$ nm [see Fig. 1(d)], indicating that the one min annealing step used after GaAs deposition is not sufficient to planarize the structure, especially for small values of d [see Fig. 1(b)].

Figure 1(g) summarizes the values of the depth of the GaAs nanoholes (top interface of GaAs QDs) and estimated QD height as a function of d. The QD height is simply estimated as the difference between the depth of $Al_{0.45}Ga_{0.55}As$ nanoholes and the depth of the subsequently GaAs-filled holes plus d. It is evident that the QD height increases almost linearly as a function of GaAs thickness.

B. Single QD spectroscopy: Evidence of bonding positive trion

The growth protocol used here offers the opportunity to tailor the optical properties, and especially the confinement energy of the QDs, via fine tuning of the growth parameters. Representative PL spectra of the ground-state emission in single QDs with different WL thicknesses are shown in Fig. 2(a). The energy axes are shifted to facilitate the comparison. As expected, the emission energy of the GaAs QDs redshifts when the WL thickness is increased as a result of increased QD height. In spite of different transition energies, the QD emission shows similar spectral features independent of d, i.e., a rather isolated emission line at high energy accompanied by other lines separated by $\gtrsim 2$ meV on the low-energy side. The high-energy peaks dominate at low excitation power and are attributed to neutral exciton recombination (X), as suggested by linear polarization-dependent measurements (see Fig. 3). In all the investigated QDs, an additional line, which dominates the spectrum at relatively high excitation power, appears on the low-energy side of X. Its energy separation from X (which is referred to as its "binding energy" E_B) shows a slight tendency to decrease with increasing GaAs WL thickness d in Fig. 2(a). The E_B values measured for several QDs in samples with different d are presented in Fig. 2(b), which shows broad distributions for each d values. Because of the absence of polarization splitting (see Fig. 3) and the p-background doping in our MBE chamber, we assign the prominent line to a positive trion X^+, as indicated by labels in Figs. 2 and 3. On the other hand, excitation-power-dependent measurements (shown later in Fig. 5) show that such a line appears at higher powers compared to the neutral exciton, letting us conclude that an extra

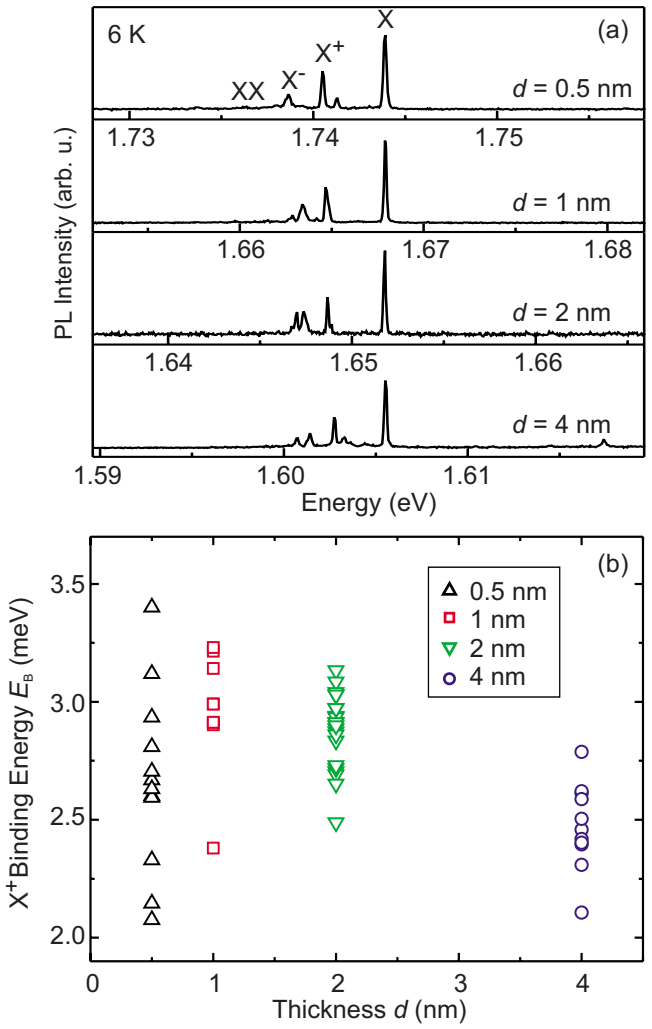

FIG. 2. (Color online) (a) Low-temperature PL spectra of representative QDs for samples of various d. The energy axes are shifted horizontally to facilitate the comparison. (b) Binding energy for the positive trion as a function of d.

carrier (possibly a hole) is not resident in the QD, but is the result of the nonresonant photogeneration process followed by carrier migration and relaxation. While PL alone is thus not sufficient to draw a definite conclusion on the origin of the peak, the calculation results presented later support its assignment to X^+. Furthermore, the positive value of E_B is fully consistent with previous studies on GaAs/AlGaAs QWs.[17]

The small features at lower energies include the negative trion X^- and other multiexcitonic species involving carriers in the QD excited states. The sharp line observed in some QDs at relatively low excitation power is attributed to X^- [see Fig. 2(a)]. As for the X^+, its binding energy tends to decrease with increasing d.

To further support the line assignment and look for signatures of the neutral biexciton (XX), we analyzed the polarization of the PL spectra for several QDs by continuous rotation of an achromatic lambda half wave plate followed by a fixed linear polarizer placed in front of the spectrometer. With the used configuration, only light polarized in the $[1\bar{1}0]$

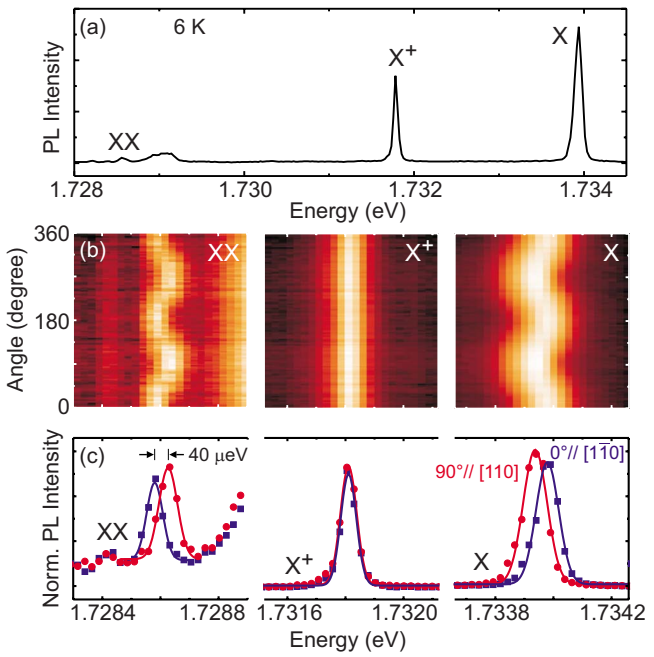

FIG. 3. (Color online) (a) PL spectrum of a QD with d =0.5 nm acquired at a polarization angle of 45°. (b) Polarization-angle-dependent PL intensity (grayscale coded) for the X, X^+, and XX lines. (c) Normalized PL spectra at polarization angle of 0° and 90° for the corresponding peaks.

crystal direction can enter the spectrometer at a polarization angle of 0°, while at 90°, light polarized along the [110] direction is selected. Representative spectra for a GaAs QD in a sample with d=0.5 nm are shown in Fig. 3. Figure 3(a) shows a PL spectrum and Fig. 3(b) the grayscale-coded PL intensity as a function of emission energy and polarization angle for the X, X^+, and XX. The X and XX lines split into two components, which are polarized perpendicular to each other. This behavior is currently ascribed to anisotropic electron-hole exchange interaction, which splits the X level into two lines.[18] Since the X state is the final state of the XX recombination, the XX emission is split by the same amount. In the left and right panels of Fig. 3(b) the X and XX lines show anticorrelated shifts, which confirm the assignment of the peak origin. The X^+ peak energy does not show any polarization angle dependence, confirming that this line originates from a singly charged exciton. Figure 3(c) shows normalized PL spectra for X, X^+, and XX at 0° and 90°. The low-energy component of X is polarized along the elongation direction of the GaAs QD (see Fig. 1), i.e., the [110] direction. The two components of X and XX in Fig. 3(c) are splitted by ~40 μeV. A systematic investigation on the role of shape anisotropy on the X splitting will be presented elsewhere.

Figure 4(a) shows the calculated binding energies of the positive and negative trions and the biexciton as functions of the thickness h [see Sec. III and bottom inset in Fig. 4(a)]. The binding energies are defined as the difference between the transition energy of a certain multiparticle complex and the neutral exciton as indicated in the inset of Fig. 4(a). The binding energy of the biexciton displays only a weak dependence on h; in contrast, the binding energy of the negative

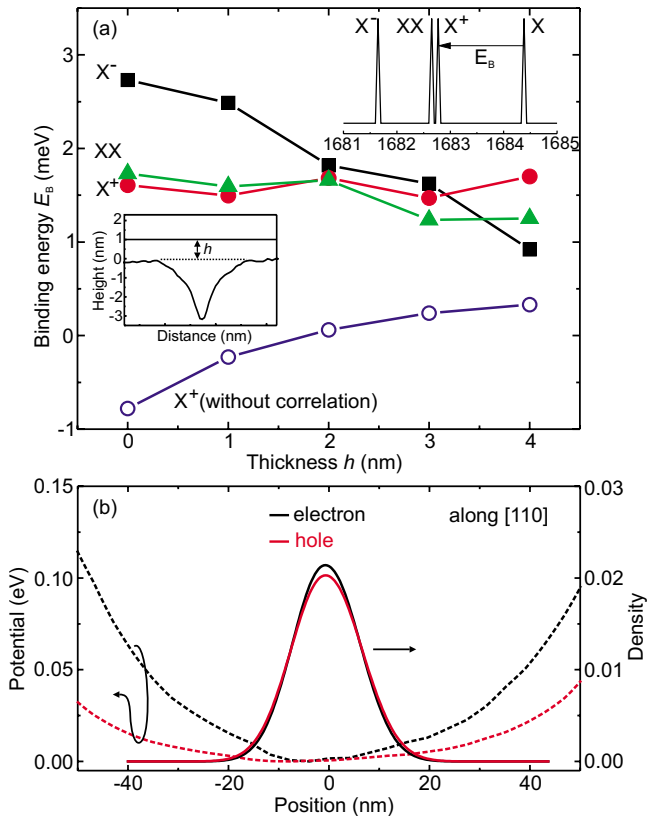

FIG. 4. (Color online) (a) Calculated binding energies of negative trion (squares), positive trion (circles), and biexciton (triangles) as a function of the WL thickness h, which is defined in the left bottom inset. The binding energies of the positive trion without taking into account the correlations (open circles) are also plotted. The top inset shows an example spectrum for $h=0$, where the binding energy for the positive trion is indicated (the energy in the horizontal axis is indicated in meV). (b) Calculated electron and hole densities (solid lines) and the effective potential (see also Fig. 8) felt by the electrons and holes (dashed lines) in the [110] direction.

trion drops substantially as h is increased. The calculated binding energy for the X^+ fluctuates with decreasing h, consistent with the experimental results [see Fig. 2(b)]. Therefore, its attribution to the positive trion emission is supported by theory. The magnitudes of the calculated binding energies, lying between 1.5 and 2 meV, however, are smaller than the observed values (between 2.5 and 3.5 meV for X^+ and around 7 meV for XX). Probably this difference is caused by an underestimation of correlation and self-consistency effects in our calculations. This discrepancy is small for the exciton and increases with the number of particles the complex is composed of. For the biexciton, for instance, Shumway *et al.*[19] observed that only 50% to 65% of the Coulomb corrections are captured by CI for a comparably sized basis set. The quantum Monte Carlo method, however, which was used as benchmark in that work, does not properly work in conjunction with eight-band $k\cdot p$ theory at present. An example of the excitonic absorption spectra, calculated for $h=0$, is shown in the top inset of Fig. 4(a).

We should point out that the binding energy of the X^+ is positive, which is usually not the case for InAs QDs (see, e.g., Ref. 20). This can be easily explained in terms of Coulomb attractions/repulsions among particles with opposite/same charges. In addition to the neutral exciton, the trion energy contains one attractive (electron-hole) and one repulsive (hole-hole) Coulomb term. Because of rather similar spatial distributions of charge densities for both electron and hole in the in-plane direction [see Fig. 4(b)], these terms have similar magnitude. The mutual correlation among particles forming the trion in a large QD slightly favors the attraction, leading to a positive binding energy. To highlight the importance of correlation effects, we present in Fig. 4(a) the binding energy of X^+ by excluding correlation effects. The binding energy is drastically reduced and becomes even negative for small values of h. Table I summarizes the contributions to the X^+ binding energy for different values of h. The binding energy $E_B(X^+)$ is the energy of the constituents (neutral exciton X and a hole) minus the energy of the complex (X^+). Denoting the single-particle energies of electron and hole as E_e and E_h, respectively, the energy of X reads $E(X)=E_e-E_h+C_{eh}+E_C(X)$, where C_{eh} is the Coulomb attraction of electron and hole and $E_C(X)$ is the correlation energy of neutral exciton. The correlation energies are estimated as differences between the CI results obtained on the basis of ten electrons and ten holes versus two electrons and two holes. The energy of X^+ reads $E(X^+)=E_e-2E_h+2C_{eh}+C_{hh}+E_C(X^+)$, where C_{hh} is the Coulomb repulsion of two holes and $E_C(X^+)$ is the correlation energy of positive trion. Finally, the binding energy of positive trion is $E_B(X^+)=-C_{eh}-C_{hh}-E_C(X^+)+E_C(X)$. A positive value of E_B has been previously observed in GaAs QWs (Ref. 17) and in II–VI QDs (see, e.g., Ref. 21), where the exciton radius may be substantially smaller than the QD lateral size.

C. QD shell structure and QDs without wetting layer

To investigate the effect of WL thickness on the shell structures of the GaAs QDs we performed excitation-power-

TABLE I. Calculated components of the binding energy of the positive trion $E_B(X^+)$ as functions of the nominal thickness of the wetting layer h.

h (nm)	C_{eh} (meV)	C_{hh} (meV)	$E_C(X^+)$ (meV)	$E_C(X)$ (meV)	$E_B(X^+)$ (meV)
0	−26.65	27.43	−5.15	−2.76	1.61
1	−23.58	23.81	−3.73	−2.00	1.50
2	−21.26	21.20	−3.36	−1.74	1.68
3	−19.41	19.17	−3.04	−1.80	1.48
4	−17.89	17.56	−3.47	−2.10	1.70

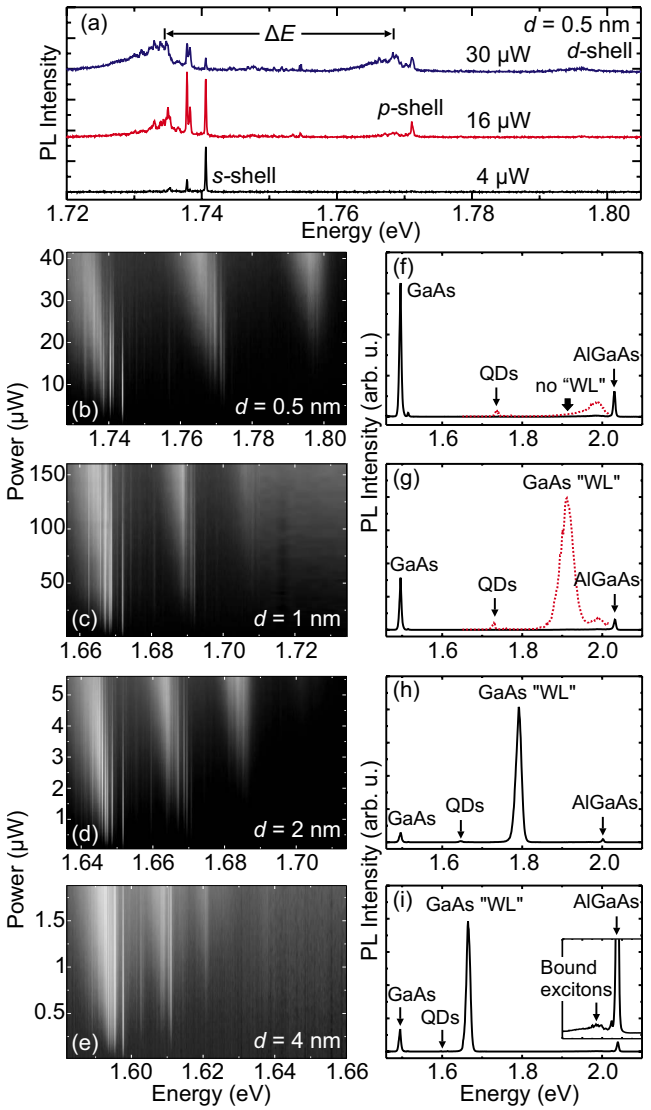

FIG. 5. (Color online) (a) PL spectra at different excitation powers for a QD with $d=0.5$ nm. Grayscale-coded PL intensity measured at 6 K as a function of excitation power and emission energy for single QDs of samples with (b) $d=0.5$ nm, (c) $d=1$ nm, (d) $d=2$ nm, and (e) $d=4$ nm. The right panel shows corresponding PL spectra collected on a wider spectral range, where the emission from bulk GaAs, QDs, GaAs WL, and $Al_{0.35}Ga_{0.65}As$ are indicated. The red dotted lines in (f) and (g) show spectra collected at very high excitation power in the energy range of 1.65–2.02 eV. The inset in (i) shows a high-resolution spectrum between 1.9 and 2.1 eV, where the emission from bound excitons in the $Al_{0.35}Ga_{0.65}As$ barrier is emphasized.

dependent PL measurements on single QDs. Representative PL spectra for a QD in the sample with $d=0.5$ nm are shown in Fig. 5(a) for different excitation powers. The intensities of neutral exciton, positively charged exciton lines, and other species saturate progressively as the excitation power rises. As a result of further increased excitation power, broad bands at the low-energy side of the neutral exciton lines emerge due to emission from multiexcitonic states. To compare the shell structure for QDs in samples with different d, we show the PL intensity as a function of excitation power and emission energy (grayscale coded) in Figs. 5(b)–5(e) for representative QDs in samples with increasing d. For each QD sample with different thicknesses d, the energy spacing between subsequent shells is approximately constant, at least for the first two excited states. The shells can be characterized by a number of nodal planes along the [110] and the $[1\bar{1}0]$ directions. The lowest shell clearly originates from s and the second from $p_{[110]}$ state. The third shell could in principle stem from $p_{[1\bar{1}0]}$ as well as from $d_{[110]}$ states. Our calculations revealed that it originates from the $d_{[110]}$ state (i.e., two nodal planes perpendicular to the [110] direction), while the shell originating from the $p_{[1\bar{1}0]}$ state has even higher energy and is not observed in the measurements. The calculated spacing energy for excitations along the $[1\bar{1}0]$ direction is almost three times higher as that along the [110] direction. Thus, in the following, we will consider only the excitations in the [110] direction.

A comparison between QDs in the four samples shows that the shell-spacing energy decreases as d increases. This observation may appear at first surprising, since the lateral extent of the QDs (which is responsible for the energy spacing between electronic levels in shallow QDs) is nominally the same in all samples. On the other hand a change in the vertical confinement potential affects the effective lateral confinement potential as discussed in more detail below.

Broad range PL spectra of the different samples are shown in Figs. 5(f)–5(i). The emission from the GaAs buffer and substrate, GaAs QDs, and $Al_{0.35}Ga_{0.65}As$ is invariably observed in all samples at a relatively low excitation power. In the sample with $d=1$ nm the emission of the AlGaAs layer is shifted to about 2.0 eV, which is ascribed to a slight deviation in the Al content (0.34 instead of 0.35) from the nominal value. The spectra are dominated by very pronounced emission from the GaAs WL in the case of $d=2$ nm and 4 nm, while only a very weak signal is observed for the sample of $d=1$ nm and no appreciable signal is observed for $d=0.5$ nm GaAs QDs. The amplified spectra at very high excitation power [red dotted spectra in Figs. 5(f) and 5(g)] show that the WL emission becomes evident for GaAs QDs of $d=1$ nm, but is still absent for the QDs of $d=0.5$ nm. In the high power spectrum of Fig. 5(f) only a weak and broad peak near the emission of $Al_{0.35}Ga_{0.65}As$ is observed. This peak is invariably observed in all the samples and is composed of many sharp lines, as shown in the inset of Fig. 5(i) for QDs with $d=4$ nm. We ascribe this emission below the band gap of $Al_{0.35}Ga_{0.65}As$ to the recombination of excitons bound to impurities or confined in alloy fluctuations.[22] Furthermore, by comparing the AFM images shown in Figs. 1(a) and 1(b) we observe that the surface gets smoother after deposition of 0.5 nm GaAs (corresponding to less than two monolayers), indicating that some of the deposited GaAs is consumed partially in planarizing the surface above $Al_{0.45}Ga_{0.55}As$. We can thus conclude that by choosing $d \lesssim 0.5$ nm we can obtain GaAs QDs without a WL connecting them, so that the next "continuum" state is represented by the bulklike top $Al_{0.35}Ga_{0.65}As$ barrier.

Figure 6 summarizes the effect of varying the WL thickness on the emission properties of QDs and WL. The blueshift in QD and WL emission for decreasing d is shown in

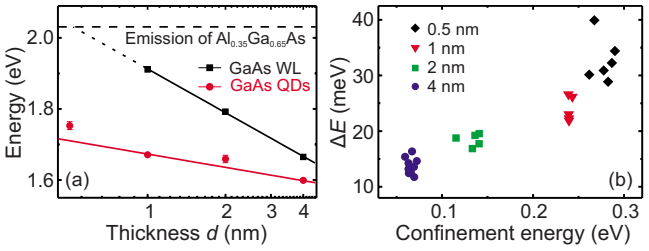

FIG. 6. (Color online) (a) Emission energy of GaAs QDs and WL for samples of various d. Solid lines are linear fits and serve as guide to the eyes. (b) Energy separation between ground state and first excited state for each sample as a function of confinement energy, which is defined by the energy difference between QDs and WL emission for each sample.

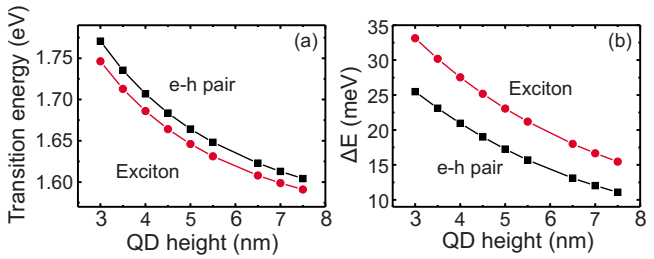

FIG. 7. (Color online) (a) Calculated energy of the lowest transition, excluding (squares) or including (circles) Coulomb interaction, as a function of QD height. (b) Calculated energy spacing between ground state and first excited-state transition, excluding (squares) or including (circles) Coulomb interaction, as a function of QD height.

Fig. 6(a), where the emission energy of the QDs is the average value found for several QDs. This trend is an obvious consequence of the decreased vertical size of QDs and WL, and can be quantitatively reproduced by our calculations (see below).

To quantify the effect of d on the energy spacing between ground state and first excited-state emission ΔE, we fitted the corresponding broad energy shells measured at high excitation power with Gaussian functions and measured the energy separation between their centers. The result of this analysis, performed on several QDs, is shown in Fig. 6(b), where ΔE is plotted as a function of the "confinement energy," defined as the energy difference between the GaAs WL and the ground-state emission of the QDs. For the sample with d $=0.5$ nm, the emission energy of the WL is replaced by that of $Al_{0.35}Ga_{0.65}As$, since no WL emission is observed. The shell energy separation shows a systematic increase from ~ 14 to ~ 32 meV, when the confinement energy is increased, pointing out to a correlation between lateral and vertical confinement potentials. This behavior is different from what is observed with other energy tuning techniques such as rapid thermal annealing.[3–5,23] In that case the blueshift in the QD emission produced by interdiffusion is accompanied by a smaller blueshift in the WL emission, so that the confinement energy decreases and so does the shell separation ΔE.

The calculated lowest transition energy and ΔE are depicted in Figs. 7(a) and 7(b), respectively, as functions of the QD height. As the height increases, all the energies of electrons, holes, and transitions decrease, as well as ΔE. These results are in good agreement with the experimental data shown in Fig. 6. While the decrease in energies is attributed to a reduced confinement energy in the growth direction, the explanation of the decreased spacing energy ΔE is at first not obvious. The spacing is related to the lateral profile of the QDs, which is not influenced by the presence of the WL. The wave functions also do not extend laterally into the WL, although they do vertically. The decrease in ΔE can be thus rationalized in the following way: due to the flat shape of the dots studied here, the lateral confinement can be approximately separated from the vertical potential allowing the separation of variables in the three-dimensional Schrödinger equation. The vertical confinement energy is obtained by solving a one-dimensional Schrödinger equation for the height of the QD at a certain point of the lateral plane. The vertical confinement energy varies laterally as the height varies, forming an effective lateral confinement potential. This reasoning elaborated in more detail can be found in Ref. 24. For smaller values of the height (e.g., when no WL is present), the dependence of the vertical energy on the height is rather steep, resulting in steep lateral potential and distant level spacings (large values of ΔE). On the contrary, for large values of the height (when a thick WL is present), the vertical energy-height dependence is rather shallow, resulting in shallow lateral potential and close level spacings (low values of ΔE). Figure 8(a) shows an example of the effective lateral confinement potential (for electrons) along the [110] direction calculated for different values h of WL thickness {the confinement along $[1\bar{1}0]$ can be approximately decoupled and does not contribute to the observed shell spacing, since all the observed shells originate in the states with nodal planes perpendicular to [110]}. The height profile was taken from an AFM image of the AlGaAs nanohole shown in Fig. 8(b), where the values of h are indicated as horizontal lines.

The effect of the Coulomb interaction on the transition energies is depicted by circles in Fig. 7. Due to the attraction between the electron and the hole forming the exciton, transition energies are reduced. This effect is more pronounced for the ground state than for the first excited state due to its lower spatial extension. The spacing ΔE, therefore, increases if the Coulomb interaction is taken into account.

The comparison of the measured and calculated transition energies and shell spacings is shown in Fig. 9(a). The points

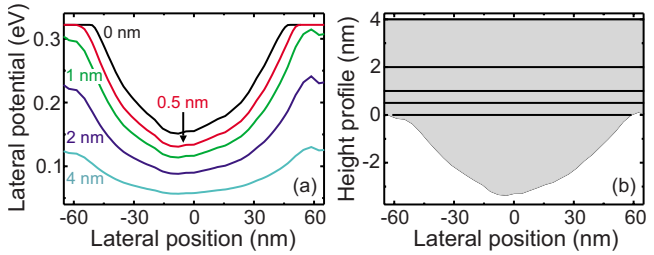

FIG. 8. (Color online) (a) Calculated effective lateral potential (for electrons) along the [110] direction for different thicknesses of WL. (b) AFM linescan of the bottom QD barrier along the [110] direction with indicated filling levels of h used for calculations.

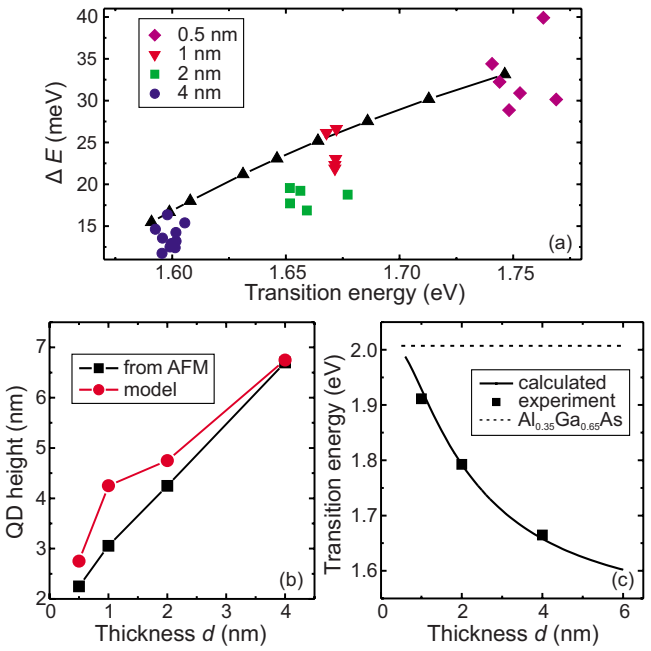

FIG. 9. (Color online) (a) Comparison of measured (symbols) and predicted (line+triangles) transition energies and ground state to excited-state separation. Different symbols correspond to different thicknesses of WL d as indicated. (b) Comparison of QD heights estimated from AFM images [see Fig. 1(g)] (squares) and heights of model structures fitted to the observed energies (circles). (c) Comparison of measured (symbols) and calculated (line) transition energies of GaAs/AlGaAs WL.

corresponding to experimental data lie in close proximity of the model line. The total heights of the QD+WL system estimated from AFM [Fig. 1(g)] are compared with the heights of the model structures as a function of d in Fig. 9(b). For the samples with $d=1$ and 2 nm, the QD height used in the model to reproduce the observed transition energies is slightly larger than the one estimated from AFM, attributed to random size fluctuations. Figure 9(c) shows calculated transition energies for the GaAs WL together with the corresponding experimental data. As pointed out in Fig. 6(a), no emission is observed for $d=0.5$ nm GaAs QDs. The calculation in Fig. 9(c) shows a very good agreement of measured [see Fig. 6(a)] and predicted transition energies for the GaAs WL. This result indicates that the thickness of the WL is not affected by the GaAs diffusion into the nanoholes due to their very low surface density.

V. CONCLUSIONS

We systematically investigated the influence of the confinement potential on the optical properties of unstrained GaAs/AlGaAs QDs with tunable WL thickness and emission energy. For fixed QD shape, a systematic decrease in the energy separation between ground and excited states is observed when the WL thickness is increased. This degree of control, which is not available for commonly studied Stranski-Krastanow QDs, is used to produce QDs without WL. Theoretical calculations of the transition energy of QDs and WL show good agreement with the experimental data and allow us to clarify the impact of the WL thickness on the optical properties of QDs. Finally, different from commonly studied InAs/GaAs QDs, the GaAs/AlGaAs QDs are characterized by a positive trion with emission energy lower than the neutral exciton, which is found to be a consequence of the large lateral extent of the QDs, and hence, of pronounced self-consistency and correlation effects. In particular, the uncommon energetic sequence of XX, X^-, X^+, and X underlines the peculiar nature of our QD system.

ACKNOWLEDGMENTS

The authors thank A. Ulhaq for his contributions to the PL measurements and S. Kiravittaya and M. Benyoucef for fruitful discussions. This work was supported by the BMBF (Grant No. 03N8711), DFG (Grant No. FOR730), and SFB (Grant No. 787). The calculations were performed using the SGI supercomputer at the HLRN Berlin/Hannover.

*lijuan.wang@ifw-dresden.de
†a.rastelli@ifw-dresden.de

[1] J. M. Garcia, T. Mankad, P. O. Holtz, P. J. Wellman, and P. M. Petroff, Appl. Phys. Lett. **72**, 3172 (1998).
[2] L. Wang, A. Rastelli, and O. G. Schmidt, J. Appl. Phys. **100**, 064313 (2006).
[3] S. Fafard and C. N. Allen, Appl. Phys. Lett. **75**, 2374 (1999).
[4] T. M. Hsu, Y. S. Lan, W. H. Chang, N. T. Yeh, and J. I. Chyi, Appl. Phys. Lett. **76**, 691 (2000).
[5] C. N. Allen, P. Finnie, S. Raymond, Z. R. Wasilewski, and S. Fafard, Appl. Phys. Lett. **79**, 2701 (2001).
[6] Y. Tu and J. Tersoff, Phys. Rev. Lett. **93**, 216101 (2004).
[7] Ch. Heyn, A. Stemmann, T. Köppen, Ch. Strelow, T. Kipp, M. Grave, S. Mendach, and W. Hansen, Appl. Phys. Lett. **94**, 183113 (2009).
[8] S. Sanguinetti, K. Watanabe, T. Tateno, M. Gurioli, P. Werner, M. Wakaki, and N. Koguchi, J. Cryst. Growth **253**, 71 (2003).
[9] A. Rastelli, S. Stufler, A. Schliwa, R. Songmuang, C. Manzano, G. Costantini, K. Kern, A. Zrenner, D. Bimberg, and O. G. Schmidt, Phys. Rev. Lett. **92**, 166104 (2004).
[10] A. Rastelli, R. Songmuang, and O. G. Schmidt, Physica E (Amsterdam) **23**, 384 (2004).
[11] S. Kiravittaya, R. Songmuang, N. Y. Jin-Phillipp, S. Panyakeow, and O. G. Schmidt, J. Cryst. Growth **251**, 258 (2003).
[12] R. Songmuang, S. Kiravittaya, and O. G. Schmidt, Appl. Phys. Lett. **82**, 2892 (2003).
[13] G. Costantini, A. Rastelli, C. Manzano, R. Songmuang, O. G. Schmidt, K. Kern, and H. V. Känel, Appl. Phys. Lett. **85**, 5673 (2004).
[14] O. Stier, M. Grundmann, and D. Bimberg, Phys. Rev. B **59**, 5688 (1999).
[15] A. Schliwa, M. Winkelnkemper, and D. Bimberg, Phys. Rev. B

79, 075443 (2009).
[16] V. Mlinar, A. Schliwa, D. Bimberg, and F. M. Peeters, Phys. Rev. B **75**, 205308 (2007).
[17] J. L. Osborne, A. J. Shields, M. Pepper, F. M. Bolton, and D. A. Ritchie, Phys. Rev. B **53**, 13002 (1996).
[18] R. Seguin, A. Schliwa, S. Rodt, K. Pötschke, U. W. Pohl, and D. Bimberg, Phys. Rev. Lett. **95**, 257402 (2005).
[19] J. Shumway, A. Franceschetti, and A. Zunger, Phys. Rev. B **63**, 155316 (2001).
[20] J. J. Finley, M. Sabathil, P. Vogl, G. Abstreiter, R. Oulton, A. I. Tartakovskii, D. J. Mowbray, M. S. Skolnick, S. L. Liew, A. G. Cullis, and M. Hopkinson, Phys. Rev. B **70**, 201308(R) (2004).
[21] H. S. Lee, A. Rastelli, M. Benyoucef, F. Ding, T. W. Kim, H. L. Park, and O. G. Schmidt, Nanotechnology **20**, 075705 (2009).
[22] M. Ramsteiner, R. Hey, R. Klann, U. Jahn, I. Gorbunova, and K. H. Ploog, Phys. Rev. B **55**, 5239 (1997).
[23] J. J. Dubowski, C. N. Allen, and S. Fafard, Appl. Phys. Lett. **77**, 3583 (2000).
[24] A. Hospodková, V. Křápek, K. Kuldová, J. Humlíček, E. Hulicius, J. Oswald, J. Pangrác, and J. Zeman, Physica E (Amsterdam) **36**, 106 (2007).